Title
Pulsed photothermal profiling of hypervascular lesions: some recent advances

Authors
Majaron, Boris
Verkruysse, Wim
Tanenbaum, BS
et al.

Publication Date
2000-05-17

DOI
10.1117/12.386236

Pulsed photothermal profiling of hypervascular lesions: Some recent advances

Boris Majaron*[a,b], Wim Verkruysse[a], B. Samuel Tanenbaum[c], Thomas E. Milner[d], J. Stuart Nelson[a]

[a] Beckman Laser Institute and Medical Clinic, Univ. of California, Irvine, CA 92162

[b] Jožef Stefan Institute, Jamova 39, SI-1000 Ljubljana, Slovenia

[c] Dept. of Engineering, Harvey Mudd College, Claremont, CA 91711

[d] Biomedical Engineering Program, University of Texas, Austin, TX 78712

ABSTRACT

Pulsed photothermal radiometry (PPTR) can be used for non-invasive depth profiling of port wine stain (PWS) birthmarks, aimed towards optimizing laser therapy on an individual patient basis. Reconstruction of laser-induced temperature profile from the experimentally obtained radiometric signal involves the skin absorption coefficient in the infrared detection band. In the commonly used 3–5 μm detection band (InSb), the absorption coefficient varies by two orders of magnitude, while assumed to be constant in the reconstruction algorithms used thus far. We discuss the problem of choosing the effective absorption coefficient value to be used under such conditions. Next, we show how to account explicitly for the strong spectral variation of the infrared absorption coefficient in the image reconstruction algorithm. Performance of such improved algorithm is compared to that of the unaugmented version in a numerical simulation of photothermal profiling. Finally, we analyze implementation of a bandpass filter which limits the detection band to 4.5–5 μm. This reduces the absorption coefficient variation to a level that permits the use of unaugmented algorithm. An experimental test of the latter approach for *in vivo* characterization of the depth of PWS lesion and epidermal thickness will be presented, including a novel technique that uses two laser excitation wavelengths in order to separate the epidermal and vascular components of the radiometric signal.

Keywords: Pulsed photothermal radiometry (PPTR), heat diffusion, imaging, image reconstruction, infrared absorption, port wine stain.

1. INTRODUCTION

Port-wine stain birthmarks (PWS) are hypervascular lesions in human skin, which consist of an excess of ectatic blood vessels. These are usually fully contained within the most superficial millimeter of the skin. The exact depth varies from patient to patient, but on average, the highest fractional blood content is found 200–400 μm below the epidermal-dermal junction.[1] PWS are currently treated by selective photocoagulation of the ectatic vasculature using a pulsed green (KTP/YAG, 532 nm) or yellow/orange laser (flashlamp-pumped dye, 577 nm, 585-600 nm). In order to optimize therapy on an individual patient basis, determination of both PWS depth and epidermal thickness is required, especially when cryogen spray cooling is applied.[2,3,4] Pulsed photothermal radiometry (PPTR), which is based on time-resolved acquisition of infrared (IR) radiant emission following pulsed laser exposure, was recently introduced for assessment of laser-induced temperature profiles in PWS.[5,6] The ability of PPTR to determine the depth of sub-surface chromophores has been demonstrated by profiling layered tissue phantoms, and by comparison with histological assessment of PWS depth.[7]

Reconstruction of laser-induced temperature profiles from experimental radiometric signals involves the value of the tissue absorption coefficient at the infrared detection wavelength. While assumed to be constant in the reconstruction algorithms developed thus far, the absorption coefficient of water, which is the primary absorber in the commonly used 3–5 μm detection

*Correspondence: 1002 Health Sciences Rd. East, Irvine; e-mail: majaron@bli.uci.edu, boris.majaron@ijs.si; fax: +1-949-824-6969

In *Lasers in Surgery: Advanced Characterization, Therapeutics, and Systems X*, R. Rox Anderson, et al., Editors, Proceedings of SPIE Vol. 3907 (2000) • 1605-7422/00/$15.00

band (InSb), varies by two orders of magnitude (Fig. 1).[8] We discuss below, how to obtain the effective value of the IR absorption coefficient under such conditions. Next, we show how to account explicitly for such strong spectral variation of the absorption coefficient in the image reconstruction algorithm. Performance of such an improved algorithm is compared to that of the unaugmented version in a numerical simulation of photothermal profiling of PWS.

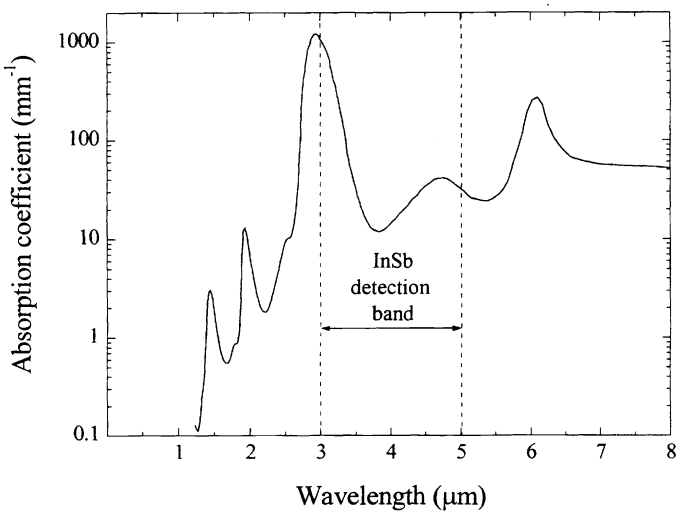

Figure 1: Infrared absorption coefficient of water, displaying a variation of two orders of magnitude within the detection band of the InSb detector (λ = 3–5 μm).[8]

Alternatively, a bandpass filter can be implemented, which narrows the IR detection band to a level that permits the use of the unaugmented algorithm. An experimental test of the latter approach using a 4.5–5 μm acquisition band for *in vivo* characterization of PWS will be presented. Note that in lesions with PWS in close proximity to the epidermal-dermal junction, epidermal heating due to broad melanin absorption may prevent determination of PWS depth, owing to limited spatial resolution of PPTR.[6,9] In order to overcome this problem, we use an approximation technique, which utilizes two laser excitation wavelengths to separate the epidermal and vascular components of the radiometric signal.[10] In this way, the epidermal thickness and PWS depth can be assessed with adequate accuracy and reliability.

2. PPTR PROFILING

2.1. Theory

The basic theory of PPTR profiling will be reviewed first.[5,6] The temperature field evolution following a pulsed laser exposure of skin can be treated by one-dimensional heat-diffusion equation (using thermal diffusivity value $D = 1.1 \cdot 10^{-7}$ m^2/s). Such an approach is reasonable, since the laser irradiated spot is typically much larger (>5 mm) than the dermal depths considered in this study (<1 mm). Using the Green's function approach, the time evolution of temperature increase $\Delta T(z,t)$ can be calculated from the initial laser-induced temperature profile $\Delta T(z',0)$ as:

$$\Delta T(z,t) = \int_{z'=0}^{\infty} \Delta T(z',0)\, K_T(z',z,t)\, dz' , \qquad (1)$$

where $K_T(z',z,t)$ represents the thermal point spread function of the problem.

Note that, owing to the finite penetration depth of the emitted infrared radiation, IR detectors do not measure the *surface* temperature. The radiometric signal obtained from a non-uniformly heated body is in general a sum of contributions from different depths z (measured from the sample surface inward):

$$S(t) = C\,\mu_{IR} \int_{z=0}^{z=\infty} B_\lambda(T(z,t))\, e^{-\mu_{IR} z}\, dz\,. \tag{2}$$

Here, constant C accounts for skin emissivity, geometry and transmission of the collection optics, sensitivity of the detector, and similar factors, μ_{IR} is the tissue absorption coefficient at the detection wavelength, and $B_\lambda(T)$ is given by Planck's law of radiation. For relatively small temperature increases encountered in our experiments, Planck's law can be linearized around the initial skin temperature T_0, resulting in

$$S(t) = C\,B_\lambda(T_0) + C\,B_\lambda'(T_0)\,\mu_{IR} \int_{z=0}^{z=\infty} \Delta T(z,t)\, e^{-\mu_{IR} z}\, dz\,. \tag{3}$$

For the discussed case of pulsed laser heating, the dynamic component of the radiometric signal $\Delta S(t)$ can now be written by inserting the temperature increase $\Delta T(z,t)$ (1) into (4), and reordering:

$$\Delta S(t) = C\,B_\lambda'(T_0)\,\mu_{IR} \int_{z'=0}^{z'=\infty} \Delta T(z',0) \int_{z=0}^{z=\infty} K_T(z',z,t)\, e^{-\mu_{IR} z}\, dz\, dz'\,. \tag{4}$$

After the point spread function of the problem $K_T(z',z,t)$ is established, integration over z can be performed, and it becomes clear that the PPTR signal (minus the background) $\Delta S(t)$ is linear in the initial temperature profile $\Delta T(z',0)$:

$$\Delta S(t) = \int_{z'=0}^{z'=\infty} K(z',t)\,\Delta T(z',0)\, dz'\,. \tag{5}$$

Definition of the kernel function $K(z',t)$ is evident from (4). In the examples below, we use a mixed (Robin) boundary condition to represent convective and radiative heat transfer at the skin surface (reduced heat transfer coefficient $h = 0.02\ \mathrm{m}^{-1}$). The kernel function then has a form:[6]

$$K(z',t) = \frac{1}{2} C\,B_\lambda'(T_0)\,\mu_{IR}\, e^{-\frac{z'^2}{4Dt}} \left\{ erfcx(u_-) + erfcx(u_+) - \frac{2h}{(h-\mu_a)} \left[erfcx(u_+) - erfcx(u_1) \right] \right\}, \tag{6}$$

where $\mathrm{erfcx}(u) = \exp(u^2)\cdot(1 - \mathrm{erf}(u))$, $u_\pm \equiv \mu_{IR}\sqrt{Dt} \pm z'/(2\sqrt{Dt})$, and $u_1 \equiv h\sqrt{Dt} \pm z'/(2\sqrt{Dt})$.

2.2. Experimental setup and methods

A PWS lesion on a volunteer patient is irradiated with a 1.5 ms long pulse from a flashlamp-pumped dye laser (ScleroPLUS, Candela, Wayland, MA), which allows a choice of four wavelengths (585 to 600 nm in increments of 5 nm). Energy density at the center of a 6 mm diameter laser spot is 5–6 J/cm^2. The transient increase in infrared radiant emission from the central 1.9×1.9 mm^2 area is recorded with an IR camera sensitive to a wavelength band of 3–5 μm (Gallileo, Raytheon, Dallas, TX), at a rate of 500 frames per second. PPTR signals $\Delta S(t)$ are obtained by calibrating the response of the camera's 64×64 array detector elements with a computer-controlled blackbody (BB701, Omega Engineering, Stamford, CT), averaging over the IR camera array, and subtracting the radiant emission level prior to the pulsed laser exposure (background).

Reconstruction of the initial temperature profile $\Delta T(z',0)$ from the experimental PPTR signals $\Delta S(t)$ is a severely ill-posed inverse problem. We solve it using a dedicated iterative algorithm based on a nonnegative-constrained conjugate-gradient method.[6] Since the PPTR signals, as well as the numerical solution in terms of the estimated initial temperature profile, are inevitably discretized, the linear mapping (5) of the initial temperature profile vector $\mathbf{T}$ ($\mathrm{T_j} = \Delta T(z_j,0)$) onto the signal vector $\mathbf{S}$ ($\mathrm{S_i} = \Delta S(t_i)$) can be represented by a kernel matrix $\underline{\mathbf{K}}$:

$$\mathbf{S} = \underline{\mathbf{K}} \cdot \mathbf{T}\,; \quad \mathrm{K_{i,j}} = K(z'_i, t_j). \tag{7}$$

The computational load is somewhat reduced by the fact that the kernel matrix elements $K_{i,j}$ have to be calculated only once for each image reconstruction example. Nevertheless, a characteristic inversion run involving a 400-element signal vector and a 64-element temperature profile vector requires a few minutes CPU time on a Sun Sparc II workstation. The computation is regularized by early termination.[6] Rather than dwelling on the issue of determining the optimal number of iteration steps, we show in the discussed example several iterative solutions, which cover the whole range from smooth, blurred temperature profiles in under-iterated solutions, near optimal and often also over-iterated solutions. As discussed previously by Milner et al.,[6] the latter display characteristic oscillations, as the algorithm attempts to fit experimental noise and other mismatches between the experimental and theoretically predicted signals.

3. SPECTRAL VARIATION OF THE ABSORPTION COEFFICIENT

3.1. Response function *R*(*z*)

In order to analyze the influence of the strong spectral variation of the IR absorption coefficient $\mu_{IR}(\lambda)$, radiometric signals must be calculated by adding radiative contributions (2) within the detection band (λ_l to λ_h):

$$\Delta S(t) = C' \int_{\lambda_l}^{\lambda_h} D(\lambda) \int_{z=0}^{z=\infty} B_\lambda'(T_0)\, \mu_{IR}(\lambda)\, \Delta T(z,t)\, e^{-\mu_{IR}(\lambda) z}\, dz\, d\lambda\,, \tag{8}$$

where we have also taken into account the spectral response of the detector $D(\lambda)$. Equation (8) can be rewritten as:

$$\Delta S(t) = C' \int_{z=0}^{z=\infty} \Delta T(z,t) \int_{\lambda_l}^{\lambda_h} D(\lambda) B_\lambda'(T_0)\, \mu_{IR}(\lambda)\, e^{-\mu_{IR}(\lambda) z}\, d\lambda\, dz = \int_{z=0}^{z=\infty} \Delta T(z,t)\, R(z)\, dz\,. \tag{9}$$

The response function $R(z)$, which is obtained by integrating over the detection wavelengths, represents the radiometric signal resulting from a unity temperature increase in a delta-layer at a depth z. In general, its functional dependence deviates from the previously assumed exponential decrease with depth (3). Figure 2 presents an example of such a response function

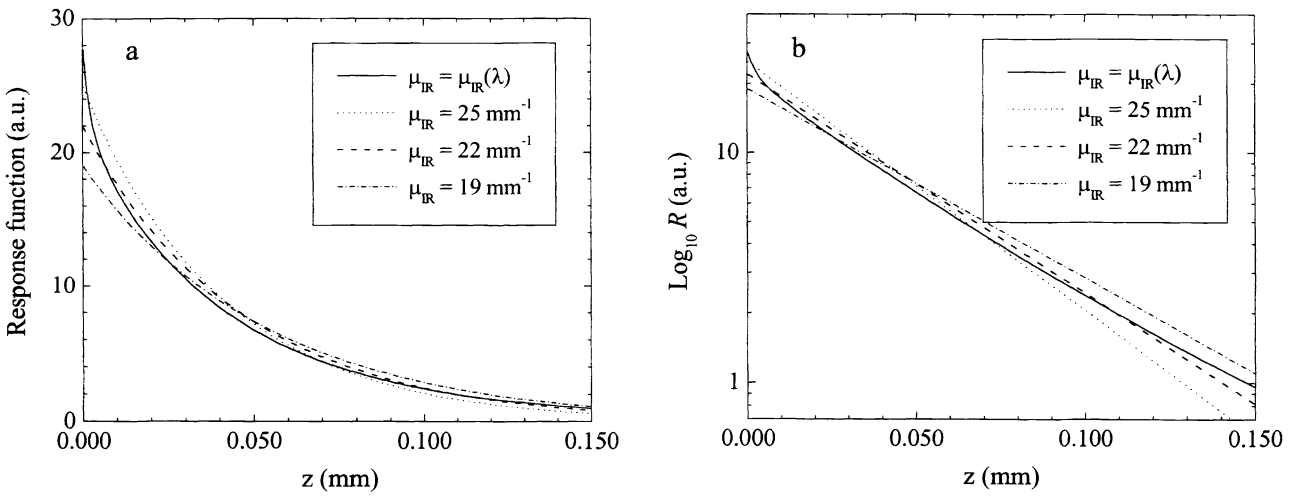

Figure 2: (a) Response function $R(z)$ calculated by taking into account the spectral variation of the IR absorption coefficient of skin (70% water content) and spectral response of the InSb detector (λ = 3–5 μm; solid curve). Response functions for various values of the spectrally constant absorption coefficient are presented for comparison (dashed and dotted curves; see the legend). (b) Same four response functions presented on a logarithmic scale, demonstrating straight lines for examples with constant μ_{IR}.

$R(z)$,calculated for $\mu_{IR}(\lambda)$ variation of skin (70% water content), detector (InSb) spectral response proportional to wavelength, 3–5 μm detection band, and initial temperature of $T_0 = 36$ °C (solid line). Three response functions obtained with various constant absorption coefficient values are also presented for comparison, displaying the exponential decay with depth (dashed and dotted lines; see the legend for values).

3.2. Effective absorption coefficient μ_{eff}

In the next step, we attempt to determine which effective value of the IR absorption coefficient μ_{IR} should be used in PPTR image reconstruction algorithms that ignore its spectral dependence within the detection band. By introducing a spectrally constant effective value μ_{eff}, integration over λ in (8) yields a constant, which can be taken out of the integral over depth z:

$$\Delta S(t) = C' \mu_{eff} \int_{\lambda_l}^{\lambda_h} D(\lambda)\, B_\lambda{}'(T_0)\, d\lambda \cdot \int_{z=0}^{z=\infty} \Delta T(z,t)\, e^{-\mu_{eff} z}\, dz \ . \tag{10}$$

By equating the response functions $R(z)$ in (9) and (10), the effective absorption coefficient value μ_{eff} is given by the implicit equation:

$$\mu_{eff}\, e^{-\mu_{eff} z} = \frac{\int_{\lambda_l}^{\lambda_h} D(\lambda)\, B_\lambda{}'(T_0)\, \mu_{IR}(\lambda)\, e^{-\mu_{IR}(\lambda) z}\, d\lambda}{\int_{\lambda_l}^{\lambda_h} D(\lambda)\, B_\lambda{}'(T_0)\, d\lambda} \ . \tag{11}$$

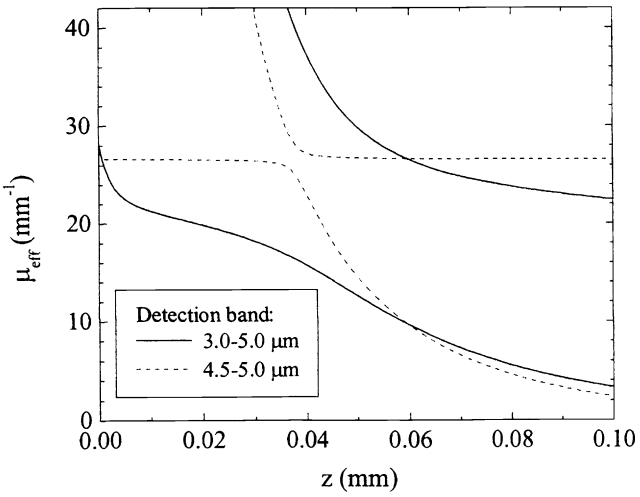

Figure 3: The effective absorption coefficient value $\mu_{eff}(z)$, as calculated from (13) for the detection band of 3–5 μm (solid line). The solution varies strongly with depth z and is double-valued for all depths. The dashed line presents the same function calculated for the detection band reduced to 4.5–5.0 μm.

The numerical solution of (11) for the 3–5 μm detection band and spectral response of the InSb detector is presented in Figure 3 (solid curves). Note that the effective absorption coefficient value μ_{eff} varies strongly with depth (z), and is double-valued. While the latter effect is intuitively quite surprising, it does not present a computational problem, as any of the two branches can evidently be used to calculate the signal from (10) (or (4)). The strong depth dependence, however, indicates that there is no constant value of μ_{eff} that would yield a correct time dependence of the PPTR signal under the discussed experimental conditions. Consequently, the reconstruction algorithm has to be augmented by taking into account the spectral dependence $\mu_{IR}(\lambda)$ according to (9) or, alternatively, the detection bandwidth should be decreased to a level that permits the use of the unaugmented algorithm. Both approaches are discussed in sections 4 and 5, respectively.

4. IMPROVED KERNEL MATRIX

In the following, we compare the performance of an image reconstruction algorithm that explicitly accounts for the spectral variation of the IR absorption coefficient $\mu_{IR}(\lambda)$ with the unaugmentedversion (using a constant value μ_{eff}). This comparison is performed in a numerical simulation of photothermal profiling. First, an initial temperature distribution $\Delta T(z',0)$ ("object") is chosen, and the corresponding PPTR signal $\Delta S(t)$ calculated using the kernel function $K(z',t)$, which involves the "correct" response function $R(z)$ (9). Then, this signal, with some noise superimposed onto it, is used as an input to the iterative image reconstruction algorithm. The reconstruction is performed first with the kernel matrix elements $K_{i,j}$ (7) calculated using the simplified response function (10) with $\mu_{eff} = 22$ mm^{-1}, and then using the correct response function $R(z)$ (9) (see Fig. 2).

Results from one such comparison are presented in Fig. 4. As the "object", we use a hyperGaussian temperature profile $\Delta T(z',0) = \Delta T_0 \exp(-2(x-x_0)^4/w^4)$ with $\Delta T_0 = 1$ °C, $x_0 = 300$ μm, $w = 100$ μm (dashed curves in Fig. 4), which vaguely resembles a laser-heated PWS layer. The corresponding signal $\Delta S(t)$, which includes also a small amount of normal noise (SNR = 1000) is calculated at 250 equidistant time points ($\Delta t = 2$ ms), and the solution (depth) space which represents the most superficial millimeter of the skin is divided into 64 intervals. As a matter of convenience, the simulation was performed on a PC (Pentium II-350), using a slightly adapted reconstruction method (details to be presented elsewhere).

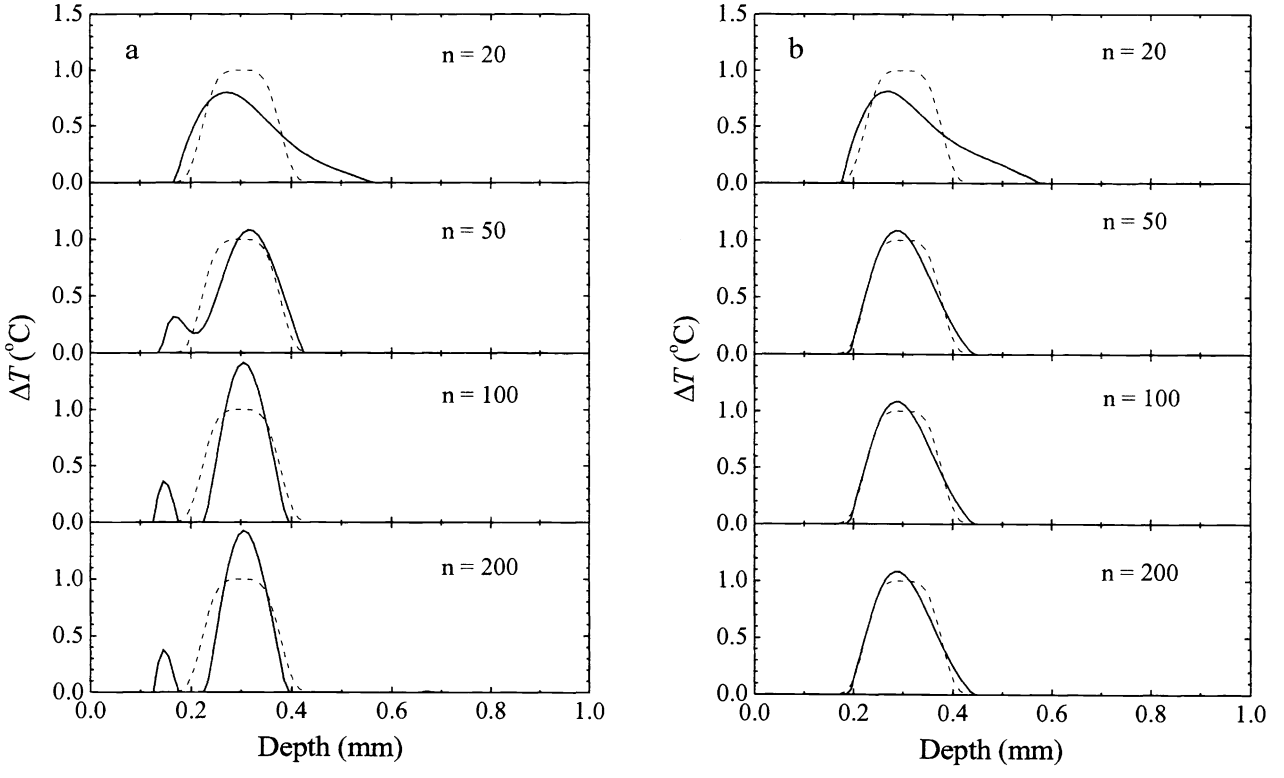

Figure 4: Convergence of the calculated temperature profile $\Delta T(z',0)$, reconstructed using the algorithm based on a constant absorption coefficient $\mu_{IR} = 22$ mm^{-1} (a), and the correct spectral dependence $\mu_{IR}(\lambda)$ (b). Solid curves represent the solution approximations obtained after 20, 50, 100 and 200 iteration steps of the image reconstruction algorithm. The hyperGaussian initial temperature profile used to calculate the input radiometric signal is plotted for comparison (dashed curves).

The under-iterated solution obtained after 20 iteration steps (n = 20) is a blurred and deformed image of the actual temperature profile, and is very similar for both approaches. When using the simplified kernel function (Fig. 4a), increasing the number of iteration steps (n) seems to temporarily improve the result, but then very rapidly produces an oscillatory

solution, which indicates the presence of an additional PWS layer starting at 120 μm – clearly a computational artifact. In contrast, the solution obtained using the corrected kernel matrix converges rapidly toward a significantly more representative image of the actual temperature profile (Fig. 4b). The position of the shallower edge of the profile, which is the most important parameter in the targeted application, is reproduced with remarkable accuracy. The peak temperature value is overestimated by only 8 %, compared to 43 % when using the simplified kernel function. The convergence of the reconstruction is also improved remarkably; when using the corrected matrix, the residual norm (which is minimized in the iteration) reaches a value of 9.6 10^{-9} after 50 iteration steps, and changes only minimally (< 1%) by iteration step 200. In contrast, with the simplified kernel function, the residue norm after 200 iteration steps is still 2.7 10^{-6} (!) - a 3 % decrease from step 100.

The difference between these two results is illustrated further in Fig. 5, where the radiometric signal calculated by each method from its last solution (n = 200) is compared to the signal used as the input to the reconstruction algorithm. Using the simplified kernel function (Fig. 5a), the mismatch between the input ("object") and predicted signal ("image") is particularly large in the first 40 ms, where the error exceeds 30 % of the signal value at that point, and 3 % of the maximal signal value overall. In contrast, with the corrected kernel function, the two signals are undistinguishable (Fig. 5b), and even the 100-times expanded residue can be hardly observed (see the inset).

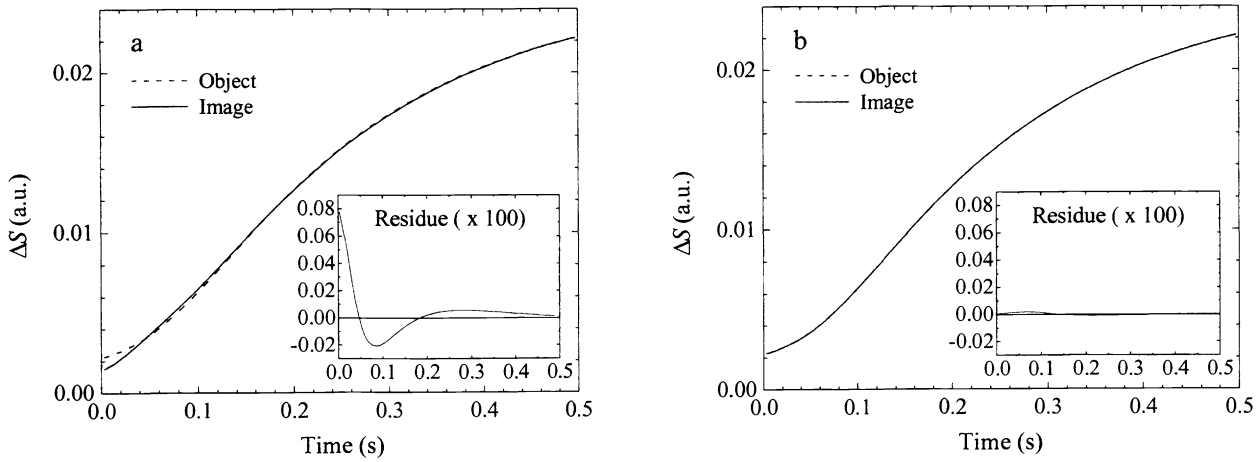

Figure 5: Radiometric signal $\Delta S(t)$, calculated from the image reconstruction solutions $\Delta T(z',0)$ obtained using $\mu_{IR} = 22$ mm^{-1} (a), and the correct spectral dependence $\mu_{IR}(\lambda)$ (b). Dashed curves represent the signal calculated from the actual initial temperature profile ("object"), which was used as the input to the reconstruction algorithm for both examples. The insets shows the residue (expanded 100 x).

Our general experience from other similar simulations is that higher levels of noise in the PPTR signal prevent successful convergence of both methods. The benefit of the corrected kernel function may thus not show up as clearly as in the presented example. This is particularly true for more complex initial temperature profiles. Nevertheless, we are confident that the performance of PPTR profiling should benefit from the suggested correction of the kernel matrix in many realistic experimental situations. In our PPTR profiling experiments, we have regularly observed a structure of the residue (similar to the one presented in the inset of Fig. 4a) well above the noise level.

5. BANDPASS FILTERING

As discussed above, an alternative approach to using the more accurate (and complex) formula in calculation of the kernel matrix elements could be a reduction of the detection bandwidth to a level that permits the use of the unaugmented algorithm. Using the equation (11), we have calculated $\mu_{eff}(z)$ for watery tissue for several detection bands. Based on the results of such an analysis, and wavelength dependence of Planck's factor $B_\lambda(T)$, we decided to reduce the detection bandwidth of our system to 4.5 – 5.0 μm. A custom long-pass IR filter (cut-on at 4.50 μm, Barr Associates, Westford MA) was fitted to the collection

optics of the InSb-array camera. As indicated by Fig. 3 (dashed curve), radiometric signals obtained with such a modified detector can be accurately described by the simplified formula (10) and effective absorption coefficient equal to $\mu_{eff} = 26.5\ mm^{-1}$. We have estimated that by using the additional filter, the amplitudes of the acquired signals $\Delta S(t)$ would decrease roughly by a factor of two. Provided that performance of the image reconstruction was limited primarily by error due to spectral variation of $\mu_{IR}(\lambda)$, rather than the level of experimental noise, such modification should improve the overall performance of PPTR profiling.

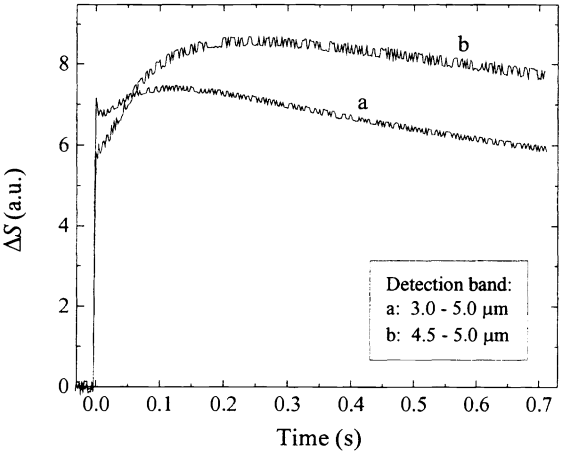

Figure 6: Comparison of PPTR signals obtained from a PWS lesion *in vivo* using: a – full detection bandwidth of the detector, and b –a detection bandwidth reduced to 4.5 – 5.0 μm. (Excitation wavelength 585 nm)

Figure 6 presents two PPTR signals obtained from the same PWS lesion on the forearm of a volunteer patient using the excitation wavelength of 585 nm, and a detection bandwidth of 3.0 – 5.0 μm (curve a), and 4.5 – 5.0 μm (b). When using the reduced detection band, the camera integration time was increased from 0.5 to 0.7 s, in order to compensate for the anticipated reduction of the radiometric signal. These two signals were used as input to the image reconstruction algorithm based on the simplified approach with a constant μ_{IR} (4). In accordance with results presented in Figs. 2a, 3, the value of $\mu_{eff} = 22\ mm^{-1}$ was used to analyze the signal "a", and $\mu_{eff} = 26\ mm^{-1}$ for signal "b".

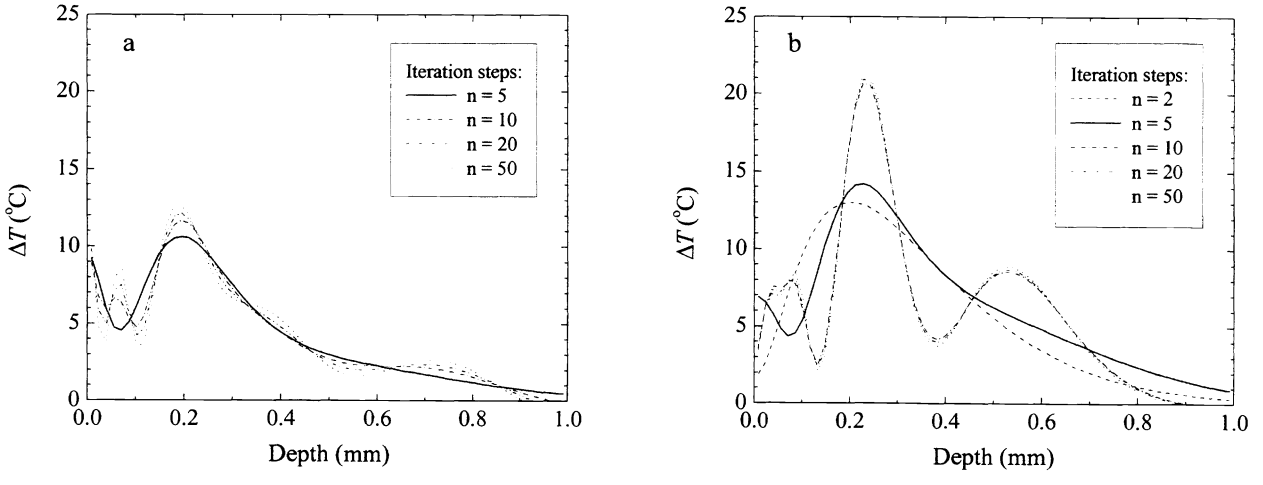

Figure 7: Longitudinal temperature profiles immediately after pulsed laser exposure of a PWS *in vivo*, as calculated iteratively from PPTR signals in Fig. 6. The excitation wavelength was 585 nm, and the detection bandwidths were 3.0–5.0 μm (a), and 4.5–5.0 μm (b).

The two families of iterative solutions (Figs. 7a, b) run from smooth, blurred temperature profiles in under-iterated solutions (see $n = 2$ in Fig. 7b), to over-iterated solutions. The latter display characteristic oscillatory artifacts, resulting from the ill-posedness of the inverse problem, combined with the experimental noise and other mismatches between the experimental and theoretically predicted signals. This is particularly pronounced in example "b", which corresponds well to the approximately two times lower SNR in the PPTR signal (Fig. 6). In both examples, the most reliable solution seems to be found after approximately five iteration steps (solid curves).

It is evident, however, that with either approach, the temperature profile in this specific PWS lesion cannot be resolved from the epidermal temperature rise, resulting from melanin absorption. This may happen when the two layers lie in close proximity to each other, and determination of PWS depth and epidermal thickness, which are required to optimize laser treatment, is thus prevented due to the limited spatial resolution of PPTR profiling. To overcome this problem, we have developed an approximation technique, which achieves improved selectivity by utilizing two excitation wavelengths.[10]

5.1. Two-wavelength excitation technique

This approximation technique allows us to differentiate between the PWS and epidermal contribution to the PPTR signal by exploring different spectral properties of the two chromophores (hemoglobin, melanin) at two excitation wavelengths. This enables determination of PWS depth and epidermal thickness even when the two layers are in close proximity to each other. Moreover, it breaks down the relatively complex initial temperature profile into two simpler "objects", which are easier to reconstruct.

The method is based on the linearity between the PPTR signal $\Delta S(t)$ and the initial temperature distribution $\Delta T(z,0)$ (5). An experimental signal obtained, for example, following pulsed irradiation at 585 nm, can thus be expressed as a sum of two components, originating from the heated PWS layer [$x(t)$], and epidermis [$y(t)$]:

$$\Delta S_{585}(t) = x(t) + y(t) . \tag{12}$$

At 600 nm, the absorption and scattering properties of the epidermis and dermis are essentially equivalent to those at 585 nm.[11] As a result, the temperature profile in the epidermis and, consequently, the corresponding signal component, is practically the same with both excitation wavelengths. In contrast, light absorption by blood at 600 nm is significantly weaker than at 585 nm.[12] This results in a lower PWS contribution to the PPTR signal obtained after 600 nm irradiation, which can therefore be approximated to the first order by

$$\Delta S_{600}(t) = \alpha\, x(t) + \beta\, y(t) . \tag{13}$$

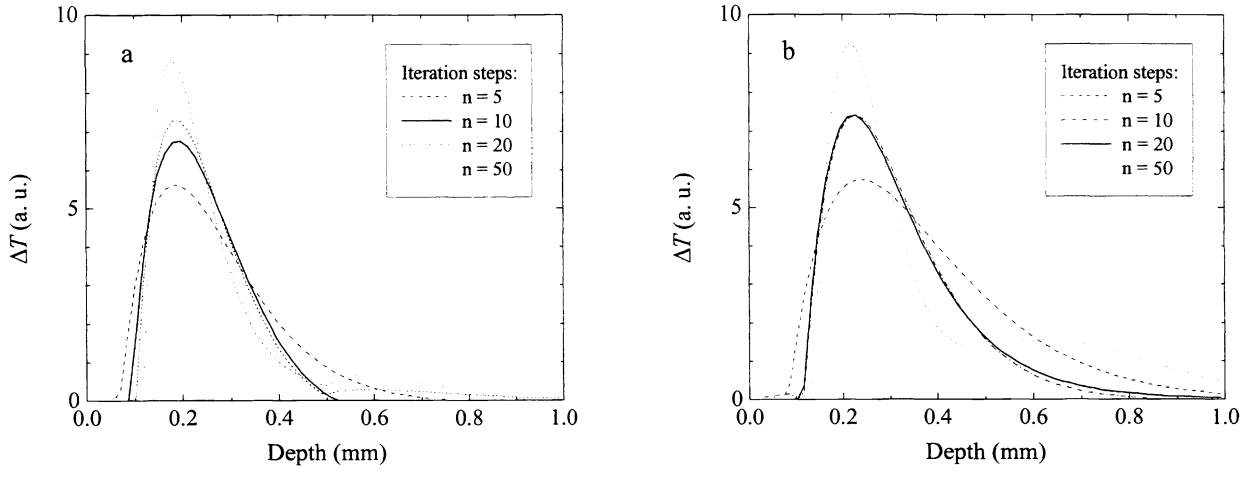

Figure 8: Non-normalized temperature profile in the PWS, as reconstructed from signals $\beta\, \Delta S_{585}(t)$ - $\Delta S_{600}(t)$ obtained using both experimental approaches (see Fig. 7 for details).

Based on the above discussed spectral properties, we can expect $\alpha < 1$ and $\beta \approx 1$.

From (12) and (13), the PWS component of $\Delta S_{585}(t)$ can be derived as

$$x(t) = \frac{\beta \Delta S_{585}(t) - \Delta S_{600}(t)}{(\beta - \alpha)}. \tag{14}$$

By using $x(t)$ as input to the image reconstruction algorithm, the temperature profile resulting exclusively from blood absorption could be obtained, but values of α and β need to be determined first. We rely on the fact that the radiometric signal immediately following pulsed irradiation results predominantly from temperature increase in the superficial layer of tissue - a few penetration depths of the detected IR radiation (40-50 μm). Since the blood vessels are located deeper in the skin, we can estimate β by requiring that the PWS signal component starts from $x(0) = 0$. A signal $\beta\, s_{585}(t) - s_{600}(t)$, proportional to $x(t)$ (14), can then be calculated. The initial temperature profile calculated from such signal is proportional to the temperature profile in PWS, and shows its top boundary very clearly (Fig. 8).

Comparison of the two examples in Fig. 8 shows that with the reduced detection band (and thus more constant μ_{IR}), the iteration can be run longer before the non-physical oscillations appear in the solution ($n = 20$ in Fig. 8b vs. $n = 10$ in Fig. 8a). Furthermore, the residual norm reaches a lower value (12.3 at steps 10 and 20, vs. 13.8 in example "a"), despite the significantly higher noise level and absolute signal level in the corresponding input PPTR signal ("b" in Fig. 6). This indicates a closer match between the theoretically predicted signal shapes and the experimentally obtained PPTR signals when using the appropriately reduced detection band. Note that, whereas the PWS depth (most superficial boundary) is the same in both examples (within the estimated accuracy of the solution), the depths of the temperature peak are significantly different (220 μm in Fig. 8b vs. 190 μm in Fig. 8a).

Similarly as above, the epidermal contribution to $\Delta S_{585}(t)$ can be derived as

$$y(t) = \frac{\Delta S_{600}(t) - \alpha \Delta S_{585}(t)}{(\beta - \alpha)}. \tag{15}$$

To determine the value of α, we use the knowledge that the pure epidermal (melanin) temperature profile must be zero at depths deeper than 150-200 μm into the skin. We therefore calculate signals $y(t)$ (15) with increasing values of α, starting

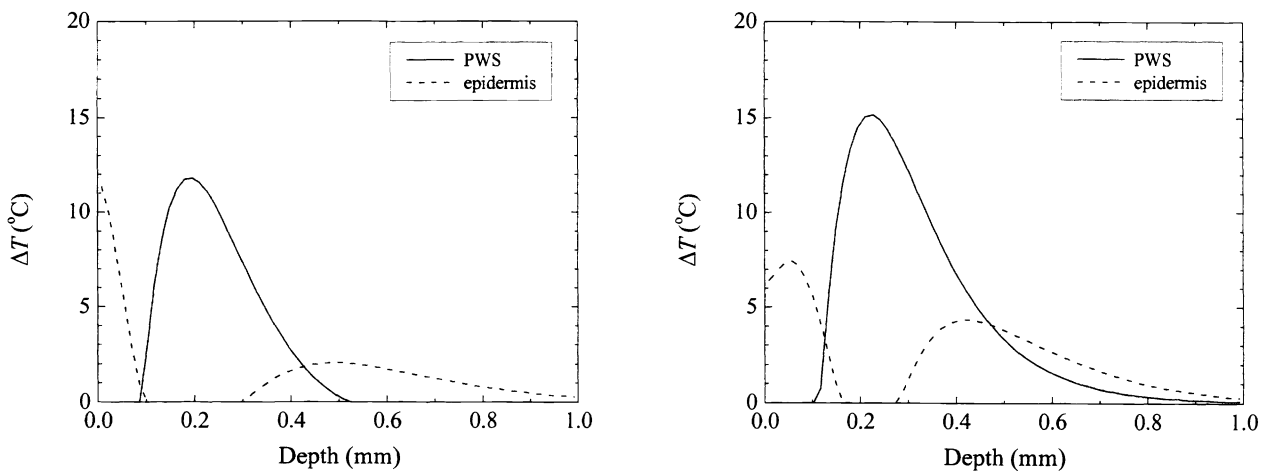

Figure 9: Initial temperature profiles in the PWS (solid line), and in the epidermis (dashed), as determined using the two-wavelength excitation technique *in vivo* and detection bandwidths of 3.0–5.0 μm (a), and 4.5–5.0 μm (b). All solutions are representative only at depths up to ~0.25 mm.

from 0, and observe the resulting temperature profiles. These usually differ little in the superficial layer, while temperatures deeper in the skin decrease monotonically with increasing α, and finally disappear. At this value of α, the solution in general oscillates less, and the residue norm reaches a lower value, than at lower (and sometimes also higher) values. Thus obtained estimate of α can then be used to renormalize the previously calculated PWS profiles.

The final result, displaying both PWS and epidermal temperature profiles, is plotted in Figure 9. The depth of the PWS most superficial boundary, which is clearly distinguished from the epidermis, is determined with reasonable accuracy. The overlap of the two profiles at ~100 μm most likely results from the uneven boundary between the epidermis and dermis, but could in part result also from broadening of one or both profiles by the reconstruction algorithm.

The epidermis profile deeper than 0.25 mm is an artifact of the method and should be disregarded. We attribute it to differences between the temperature profiles induced in PWS with 585 vs. 600 nm irradiation. Since the latter penetrates deeper into the PWS lesion, the validity of proportionality between the two PWS temperature profiles, assumed in (13), deteriorates with depth. However, such a first order approximation definitely holds in the thin top layer of the PWS, where both temperature profiles (using 585 and 600 nm excitation) can be linearized. The solutions presented in Fig. 9 are thus representative up to a depth of ~0.25 mm. At greater depths, the PWS profile solution may differ from the actual temperature profile induced by the 585 nm excitation, as some contribution from deeper blood vessels is contained in signal $y(t)$. More experimental examples and a thorough discussion of the strengths and limitations of this approach will be presented elsewhere.[10]

6. CONCLUSIONS

PPTR can be used for non-invasive depth profiling of PWS, with a potential for on-line guidance of laser therapy on an individual patient basis. In reconstruction of the laser-induced temperature profiles from the experimentally obtained radiometric signals, variation of the tissue absorption coefficient within the commonly used 3–5 μm IR detection band (InSb) has to be taken into account when calculating the kernel function of the problem. Alternatively, a bandpass filter can be implemented to reduce the absorption coefficient variation in the detection band and allow the use of the simplified kernel function. The epidermal and PWS contributions to the PPTR signals can be separated using two laser excitation wavelengths, which enables determination of the epidermal thickness and PWS depth *in vivo*, even when the two layers are in close physical proximity to each other.

7. ACKNOWLEDGEMENT

This work was supported by a research grant from the Institute of Arthritis and Musculoskeletal and Skin Diseases (AR43419) at the National Institutes of Health, and by the Slovenian Ministry of Science and Technology (BM). Institutional support from the Office of Naval Research, Department of Energy, National Institutes of Health, and the Beckman Laser Institute and Medical Clinic Endowment is also acknowledged.

7. REFERENCES

1. S. H. Barsky, S. Rosen, D. E. Geer, and J. M. Noe, "The nature and evolution of port wine stains: a computer-assisted study," *J. Invest. Dermatol.* **74**, pp. 154-157, 1980.
2. B. Anvari, T. E. Milner, B. S. Tanenbaum, S. Kimel, L. O. Svaasand, and J. S. Nelson, "Selective cooling of biological tissues for thermally mediated therapeutic procedures," *Phys. Med. Biol.* **40**, pp. 241-252, 1995.
3. B. Anvari, B. S. Tanenbaum, T. E. Milner, S. Kimel, L. O. Svaasand, and J. S. Nelson, "A theoretical study of the thermal response of skin to cryogen spray cooling and pulsed laser irradiation: implications for the treatment of port wine stain birthmarks," *Phys. Med. Biol.* **40**, pp. 1451-1465, 1995.
4. W. Verkruysse, B. Majaron, B. S. Tanenbaum, J. S. Nelson, "Optimal cryogen spray cooling parameters for pulsed laser treatment of port wine stains," submitted to *Lasers Surg. Med.*

5. S. L. Jacques, J. S. Nelson, W. H. Wright, and T. E. Milner, "Pulsed photothermal radiometry of port-wine-stain lesions," *Appl. Opt.* **32**, pp. 2439-2446, 1993.
6. T. E. Milner, D. M. Goodman, B. S. Tanenbaum, and J. S. Nelson, "Depth profiling of laser-heated chromophores in biological tissues by pulsed photothermal radiometry," *J. Opt. Soc. Am.* **A 12**, pp. 1479-1488, 1995.
7. T. E. Milner, D. J. Smithies, D. M. Goodman, A. Lau, and J. S. Nelson, "Depth determination of chromophores in human skin by pulsed photothermal radiometry," *Appl. Opt.* **35**, pp. 3379-3385, 1996.
8. E. D.Palik ed., *Handbook of Optical Constants in Solids II*, Academic Press, 1991.
9. D. J. Smithies, T. E. Milner, B. S. Tanenbaum, D. M. Goodman, and J. S. Nelson, "Accuracy of subsurface distributions computed from pulsed photothermal radiometry," *Phys. Med. Biol.* **43**, pp. 2453-2463, 1998.
10. B. Majaron, W. Verkruysse, B. S. Tanenbaum, T. E. Milner, S. A. Telenkov, D. M. Goodman, and J. S. Nelson, "Combining two excitation wavelengths for pulsed photothermal profiling of hypervascular lesions in human skin," submitted to *Phys. Med. Biol.*
11. S. Wan, R. R. Anderson, and J. A. Parrish, "Analytical modeling for the optical properties of the skin with in vitro and in vivo applications," *Photochem. Photobiol.* **34**, pp. 493-499, 1981.
12. E. J. van Kampen and W. G. Zijlstra, "Determination of hemoglobin and its derivatives", in *Advances in Clinical Chemistry*, H. Sobotka and C. P. Stewart, eds., (Academic Press, New York, 1965), p. 158.